CARBON 46 (2008) 501–510

available at www.sciencedirect.com

ScienceDirect

journal homepage: www.elsevier.com/locate/carbon

Overcoming the barrier to graphitization in a polymer-derived nanoporous carbon

Christopher L. Burket[a], *Ramakrishnan Rajagopalan*[b], *Henry C. Foley*[a,b,c,*]

[a]*Department of Chemical Engineering, The Pennsylvania State University, University Park, PA 16802-4400, United States*
[b]*Materials Research Institute, The Pennsylvania State University, University Park, PA 16802-4400, United States*
[c]*Department of Chemistry, The Pennsylvania State University, University Park, PA 16802-4400, United States*

ARTICLE INFO

Article history:
Received 10 July 2007
Accepted 17 December 2007
Available online 29 January 2008

ABSTRACT

A new pathway to synthesize a carbon with both nanoporosity and pre-graphitic structures has been discovered by annealing at 2000 °C a CO_2 activated, non-graphitizing, nanoporous carbon originally derived from polyfurfuryl alcohol. The activation process with CO_2 overcomes the barrier to graphitization normally present in this carbon even when treated at high temperature. Gas adsorption analysis, skeletal density measurements, X-ray diffraction, and transmission electron microscopy are utilized to probe the structure of both the non-activated and the activated carbons at 800, 1200, 1800, and 2000 °C. The influence of activation time is also examined. Prior to activation the nanopore walls are comprised of several layers of disordered graphenes. Activation eliminates the barrier to graphitization by reducing the number of layers below the limit of detection and by removing carbon material highly susceptible to oxidation. Annealing at 2000 °C of the carbon activated to 84% burnoff induces the formation of pre-graphitic domains amongst the nanoporous carbon. The (002) bands corresponding to $2\theta = 24.3°$, 26°, and 26.5° are identified and assigned to amorphous, turbostratic, and graphitic morphologies. A pore volume of 0.50 $cm^3\ g^{-1}$ localized in pores below 2 nm in size is preserved after annealing.

1. Introduction

Polymer-derived carbons are considered to be either graphitizing or non-graphitizing depending on their tendency to undergo transformation to graphite when annealed at temperatures above 1000 °C [1,2]. Non-graphitizing carbons, such as that derived from polyfurfuryl alcohol (PFA), are *globally* amorphous, meaning that on average they are disordered and non-crystalline even though there may be small regions that are more ordered locally. Although non-crystalline, they are *regular* solids meaning that they consist of structural elements of the same kinds chaotically arranged in space. Among the most notable features of these carbons that points to their regularity is that they have pores which are mostly in a range below 1.0 nm, and usually narrowly distributed around an average of 0.5 nm. These pore sizes are very close to those of zeolites, especially H-ZSM-5 and related structures. As a result small molecules can be separated on the basis of size or shape either by complete exclusion or by differing rates of transport [3–6]. As a result, in the past these carbons have been referred to as carbon molecular sieves. Although the pores are often quite narrowly distributed around a mean of 0.5 nm, depending on the conditions of preparation from polymerization to pyrolysis some of the

* *Corresponding author:* Address: Department of Chemical Engineering, The Pennsylvania State University, University Park, PA 16802-4400, USA. Fax: +1 814 865 5604.
E-mail address: hcf2@psu.edu (H.C. Foley).
0008-6223/$ - see front matter © 2007 Elsevier Ltd. All rights reserved.
doi:10.1016/j.carbon.2007.12.016

pores have sizes extending out to 2.0 nm, for this reason we refer to these materials as nanoporous[1] carbons (NPC)[7].

Another remarkable feature of the NPCs is that they are quite thermally stable, and resistant to chemical attack. These two features are of great practical as well as fundamental interest. Practically, in a subset of growing applications involving water, acidic media, and hydrofluoric acid the NPC materials can be deployed successfully as catalyst supports, catalysts in their own right, or as selective adsorbents whereas under the same condition a zeolite molecular sieve would be unstable. On a more fundamental level the unique properties of the NPC material have been attributed to the presence of extensive cross-linking in the precursor, which manifests as a chaotic misalignment of defective graphene layers in the carbon [8–11]. Over the last sixty years, a wealth of knowledge has been accumulated with respect to the structure and properties of non-graphitizing carbon. One of the most intriguing manifestations of cross-linking, besides the development of regular nanopores, is the resistance of these materials to graphitization even at elevated temperatures (2000 °C). As of yet the intrinsic nature of this barrier to graphitization is still not understood. In this paper we report on a new reaction pathway that allows us to circumvent the barrier and which gives us deeper insight into the basis for the resistance to graphitization.

Multiple models for the structures of non-graphitizing carbons exist. Rosalind Franklin proposed randomly oriented graphite crystallites connected by disordered carbon sheets [1]. Jenkins and Kawamura suggested a three-dimensional network of curved graphitic ribbons, or microfibrils, which loop around each other with no preferred orientation [2]. Dahn et al. described a "falling cards model", wherein the cards are graphene sheets stacked in a random manner [12]. Additionally, Harris envisioned the carbon as a collection of multilayered fullerene-like fragments [13,14]. In each scenario the solid contains thermally stable constituents composed of carbon; in the more recent models these structural units also include curvature that arises from defects in the hexagonal lattice and cross-links between the layers. It is known that curvature is forced into a sheet of six-membered rings by introducing five and seven-membered rings. The effect has been demonstrated by simulation and verified experimentally [15–17]. The barrier which blocks the pathway to the formation of highly-ordered graphite, the thermodynamically favored allotrope, and the formation of regular nanopores we believe are both related to the inherent broken structural symmetries produced from defects formed during pyrolysis and which are partially stabilized by induced curvature.

The effect of annealing on a graphitizing carbon has been studied in detail by Rouzaud and Oberlin [11]. The carbon microstructure passes through four phases during conversion to graphite. Pyrolysis creates stage one, where the carbon is comprised of aromatic domains, deemed basic structural units (BSU). Stage two is achieved by removal of labile heteroatoms, which allows alignment of the BSU along the *c*-axis to form imperfectly stacked distorted columns. Inter-layer defects are annealed out of the structure during stage three, leaving turbostratic graphite with wrinkled planes. Removal of heteroatoms fixed at the defects in the layers permits the defects to heal and form highly crystalline graphite. The same four transformations are also expected to occur in non-graphitizing carbon, but they take place to a much lesser degree and without large scale graphitization. The implication is that movement of the BSU, required for gross graphitization, is restricted by cross-linked structures formed in the early stages of polymerization.

Graphitization of non-graphitizing carbon, does occur, however, in the presence of a variety metals [18–21]. If inorganics contaminate the carbon, then they can catalytically induce graphitization upon annealing. Similarly, stress can induce graphitization of pure carbon, as has been reported for temperatures in excess of 2000 °C [22,23]. However, in these cases the resulting carbons are non-porous. For new applications such as ultracapacitors, it would be advantageous to have a combination of nanopores and graphitic carbon to provide high surface area and low resistance. Hence a practical and fundamental challenge exists in finding a reaction path that can retain porosity while also inducing graphitization.

The current study follows the evolution of porosity and microstructure in NPC and activated NPC (a-NPC) between 800 and 2000 °C by gas sorption analysis, skeletal density measurements, X-ray diffraction (XRD), and transmission electron microscopy (TEM). Evidence of a reduction in the barrier to graphitization is found in a-NPC.

2. Experimental

2.1. *Synthesis of polyfurfuryl alcohol and nanoporous carbon*

p-Toluenesulfonic acid monohydrate (0.048 g) (Sigma–Aldrich) was dissolved in 5 ml of Triton X-100 (Sigma–Aldrich) by heating mildly. To this solution, 5 ml of furfuryl alcohol (FA, 99% Sigma–Aldrich) was added. The reaction mixture was stirred magnetically at 10 °C. After polymerization for 48 h the product was transferred to a quartz boat and pyrolyzed under flowing argon in a quartz tube furnace. The sample was heated at a rate of 10 °C min^{-1} to 800 °C and held for 1 h . Thermogravimetric analysis of Triton X-100 indicated no organic or inorganic residue after pyrolysis. The carbonaceous material is pure and derived entirely from the polyfurfuryl alcohol. The carbon was ground and sieved to a particle size of <38 μm.

Activated NPC was prepared in a quartz tube furnace. Carbon (0.5 g) was heated to 900 °C over 1 h in flowing argon. After 1 h of soak time the gas was switched to CO_2 and soaked up to 84% burnoff. The sample was cooled back to room temperature under argon. The entire experiment was conducted at atmospheric pressure.

High temperature treatment (HTT) was carried out in a Red Devil furnace (R.D. Webb Company, Natick, MA). The hot zone was evacuated to 10^{-3} mbar for 24 h prior to annealing, then backfilled to atmospheric pressure with argon. A 25 °C min^{-1} heating rate was employed with a 1 h soak at temperatures between 1200 and 2000 °C.

[1] The width of a nanopore does not exceed 2 nm. The IUPAC term for a pore of this dimension is micropore.

2.2. Characterization of nanoporous carbon

A methyl chloride adsorption isotherm was used to calculate the total pore volume and the average pore size of the carbons according to the Horvath–Kawazoe and the Kelvin models in the nano- and mesopore regions respectively [24]. A slit pore shape was assumed for pores less than 0.7 nm. The diameter of the methyl chloride probe molecule was taken to be 0.418 nm. The skeletal density of the carbons was measured by gas displacement of helium on an AccuPyc 1330 (Micromeritics, Norcross, GA). The apparent surface area of the carbons was calculated from the N_2 isotherm measured on a Gemini 2370 (Micromeritics, Norcross, GA) and the BET equation.

XRD patterns were collected on a Scintag Pad V X-ray powder diffractometer using CuKα radiation with a step size of 0.01° 2θ and a count time of 0.5 s. Acquisition conditions were 35 kV and 30 mA. A NIST SRM 640c silicon standard was used to correct the line position and broadening of the carbon patterns.

Samples for TEM were prepared by grinding the carbon, dispersing in ethanol, and placing a drop on a lacey carbon grid. Images were gathered on a JEOL 2010F 200 keV field emission microscope. The sample was observed in numerous regions; the images shown are representative of the whole of the sample.

3. Results

Samples are labeled according to the maximum temperature of HTT and burnoff due to activation was noted. For example, NPC1200 was annealed at 1200 °C and a-NPC1200/84 was activated to 84% burnoff prior to annealing.

A plot of the total pore volume of NPC800, as measured by methyl chloride adsorption, is given in Fig. 1. The carbon had a pore volume of 0.20 $cm^3\ g^{-1}$, with a nearly monodisperse set of nanopore sizes at a width of ~0.5 nm. A small amount of mesoporosity was also present. Annealing at 1200 °C rendered a majority of the nanopores inaccessible to the probe gas. Just 10% of the original pore volume remained at 2000 °C. The volumes of the nano- and mesopores are summarized in Table 1 in addition to the apparent carbon surface areas measured by N_2 BET. The errors associated with the non-activated and activated apparent surface area measurements are 11 and 52 $m^2\ g^{-1}$, respectively.

Table 1 – Nano- (V_{nano}), meso- (V_{meso}) and total pore (V_{total}) volumes, and apparent surface areas (SA) of NPC and a-NPC

Sample	V_{nano} ($cm^3\ g^{-1}$)	V_{meso} ($cm^3\ g^{-1}$)	V_{total} ($cm^3\ g^{-1}$)	Apparent SA ($m^2\ g^{-1}$)
NPC800	0.16	0.04	0.20	317
NPC1200	0.04	0.04	0.08	23
NPC1800	0.01	0.00	0.01	27
NPC2000	0.01	0.02	0.03	22
a-NPC800/84	0.95	0.35	1.30	2135
a-NPC1200/84	0.84	0.26	1.10	1967
a-NPC1800/84	0.57	0.25	0.82	1698
a-NPC2000/84	0.50	0.22	0.72	1060

Burnoff is 84% for a-NPC800.

Fig. 2 illustrates the changes in skeletal density occurring as NPC and a-NPC/84 are subjected to HTT. The density of NPC800 was 1.93 g cm^{-3}. For non-activated samples the density was not significantly altered up to 1400 °C, at which point it began to decrease towards a value of 1.40 g cm^{-3} at 2000 °C. Activation to 84% burnoff increased the density to 2.35 g cm^{-3} for a-NPC800/84, which is slightly higher than the maximum density of graphite. It is important to consider the potential for significant helium adsorption in nanoporous carbons, which may lead to errors in the measurement of skeletal density [25]. However, the increased apparent density values after activation are clearly indicative of opening of closed pores in these carbons. When subjected to HTT, the a-NPC/84 density decreases linearly. At 2000 °C the density of a-NPC2000/84 remains 0.56 g cm^{-3} higher than NPC2000.

Powder X-ray diffraction patterns were collected for each NPC sample and are depicted in Fig. 3. NPC800 was characterized by a broad (002) line, which was indicative of a high

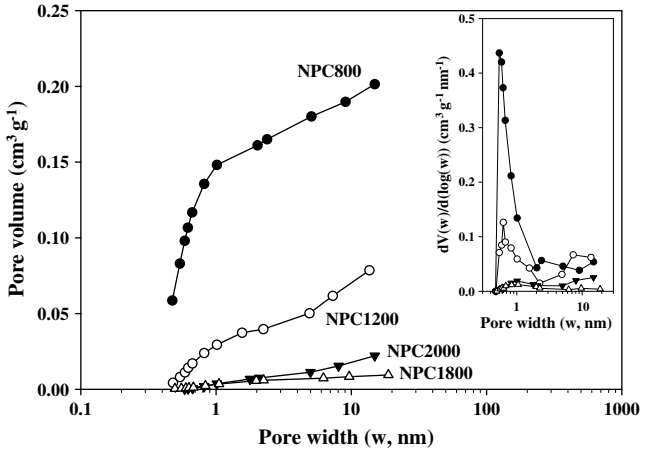

Fig. 1 – Total and differential pore volumes of NPC800, NPC1200, NPC1800, and NPC2000, as calculated by the methyl chloride adsorption isotherm.

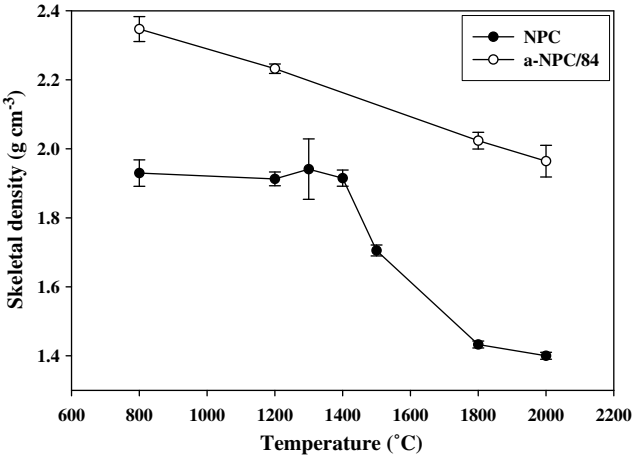

Fig. 2 – Skeletal densities of NPC and a-NPC/84 versus annealing temperature.

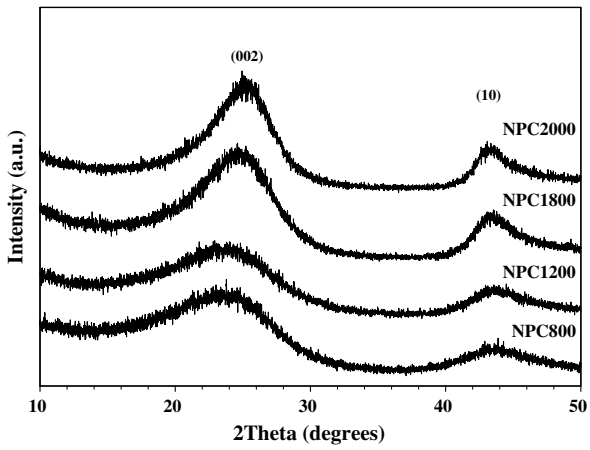

Fig. 3 – XRD patterns of NPC800, NPC1200, NPC1800, and NPC2000.

degree of disorder in the graphenes. As HTT continued at progressively higher temperatures the peak narrowed and shifted towards the ideal (002) 2θ value of graphite, 26.5°. The d_{002} of NPC800 was calculated from the Bragg equation and was found to be 3.68 Å. No change was observed at 1200 °C and the d_{002} narrowed to 3.55 and 3.50 Å with HTT at 1800 and 2000 °C. An average crystallite size was determined by the Scherrer equation using the (002) and (10) peaks for L_c and L_a, respectively. L_c was found to increase from 10 to 15 Å between 800 and 2000 °C. L_a increased from 15 to 27 Å over the same temperature range. All values of d_{002}, L_c, and L_a are summarized in Table 2.

Changes in microstructure were also observed via TEM; images are shown in Fig. 4. NPC800 was homogeneous and clearly globally amorphous. Ordered domains appeared and the number of stacked layers increased as a function of HTT. NPC2000 was inhomogeneous and comprised of highly curved ribbons no more than 10 graphenes in thickness.

Activation of NPC800 with CO_2 to 84% burnoff produced the carbon a-NPC800/84. The activated carbon was then subjected to HTT. A total and differential pore volume was measured at each temperature. The results are summarized in Fig. 5 and Table 1. A six-fold increase in nanopore volume to 0.95 $cm^3\ g^{-1}$ was realized upon activation. As HTT increased, the nanopore volume was reduced. The nanopore volume of a-NPC2000/84 was 0.50 $cm^3\ g^{-1}$. There was relatively very little change in the pore volume between a-NPC1800/84 and a-NPC2000/84. The differential pore volume demonstrated a shift in the mean nanopore width from 0.5 to 0.82 nm after activation, which was not altered by subsequent annealing.

Table 2 – Interlayer spacing (d_{002}), and crystallite sizes (L_c and L_a) for components of NPC and a-NPC

Sample	Component	d_{002} (Å)	L_c (Å)	L_a (Å)
NPC800	A	3.69	10	15
NPC1200	A	3.69	10	18
NPC1800	A	3.55	13	24
NPC2000	A	3.50	15	27
a-NPC800/84	A	–	–	17
a-NPC1200/84	A	–	–	18
a-NPC1800/84	A	3.72	5	24
a-NPC2000/84	A	3.66	10	25
	T	3.44	276	
	G	3.37	145	

L_a was calculated from the (10) peaks.

X-ray diffraction patterns for the annealed a-NPC/84 samples are given in Fig. 6. The (002) reflection was absent from a-NPC800/84, which indicated the number of graphenes in the pore wall were reduced below the level of detection. A broad (002) line reappeared in a-NPC1800/84, denoting coalescence of graphenes into thicker stacks. A surprising pattern was observed when the HTT was increased further to 2000 °C; a sharp (002) line appeared superimposed on the broad background. The d_{002}, L_c, and L_a values were calculated and are given in Table 2.

The (002) peak of a-NPC2000 was resolved into an amorphous (A), turbostratic (T), and graphitic (G) component [26,27]. The fit is shown in Fig. 7. The A-component had a d_{002} of 3.66 Å, with an L_c size of 10 Å. A d_{002} of 3.44 Å identified the T-component. Its average L_c size was 276 Å. The G-component had a 3.37 Å d_{002} and 145 Å L_c. The trend in L_a was similar to the non-activated samples.

The microstructures of a-NPC800/84 and a-NPC2000/84 are shown in Fig. 8. a-NPC800/84 was confirmed to be amorphous in Fig. 8a and no changes were observed at 1200 or 1800 °C. Two distinct microstructures were found after HTT at 2000 °C. Fig. 8b demonstrates an amorphous structure, while Fig. 8c displays pre-graphitic textures. Fig. 8d shows the A-, T-, and G- component microstructures in intimate contact.

In order to determine the effect of activation time on the formation of pre-graphitic structures at 2000 °C, samples of NPC800 were activated for 0.5, 1.5, and 2.5 h, in addition to the standard 3.5 h described previously. The carbon burnoffs were 15%, 42%, and 69% for 0.5, 1.5, and 2.5 h, respectively. The cumulative and differential pore volumes for the activated carbons are given in Fig. 9. A slight increase in nanoporosity was observed after 15% burnoff. A marked increase in nanoporosity was found after 42% and 69% of activation. Between 69% and 84% burnoff the porosity increased, although it was primarily in the mesopore range. Skeletal densities were also recorded as a function of activation time. The values are shown in Fig. 10.

Fig. 11 shows the X-ray diffraction patterns collected for each of the carbons activated to less than 84% burnoff. The broad (002) peak of NPC800 was maintained at 15% of activation. The intensity was reduced at 42% and the peak was indistinguishable from the baseline beyond 69%. The d_{002}, L_c, and L_a parameters for the samples were relatively constant regardless of the activation time. The values are summarized in Table 3.

The porosity retained by each of the activated carbons after HTT at 2000 °C is demonstrated in Fig. 12. Pore volumes of 0.55 and 0.72 $cm^3\ g^{-1}$ were maintained in the 69% and 84% samples, respectively. For the a-NPC2000/42 carbon 0.14 $cm^3\ g^{-1}$ of pore volume was present, which was nearly equivalent to the initial pore volume of NPC800 prior to activation or HTT. The sample activated to 15% burnoff was rendered almost non-porous after annealing at 2000 °C. This suggests that the activation time was inadequate to develop a pore vol-

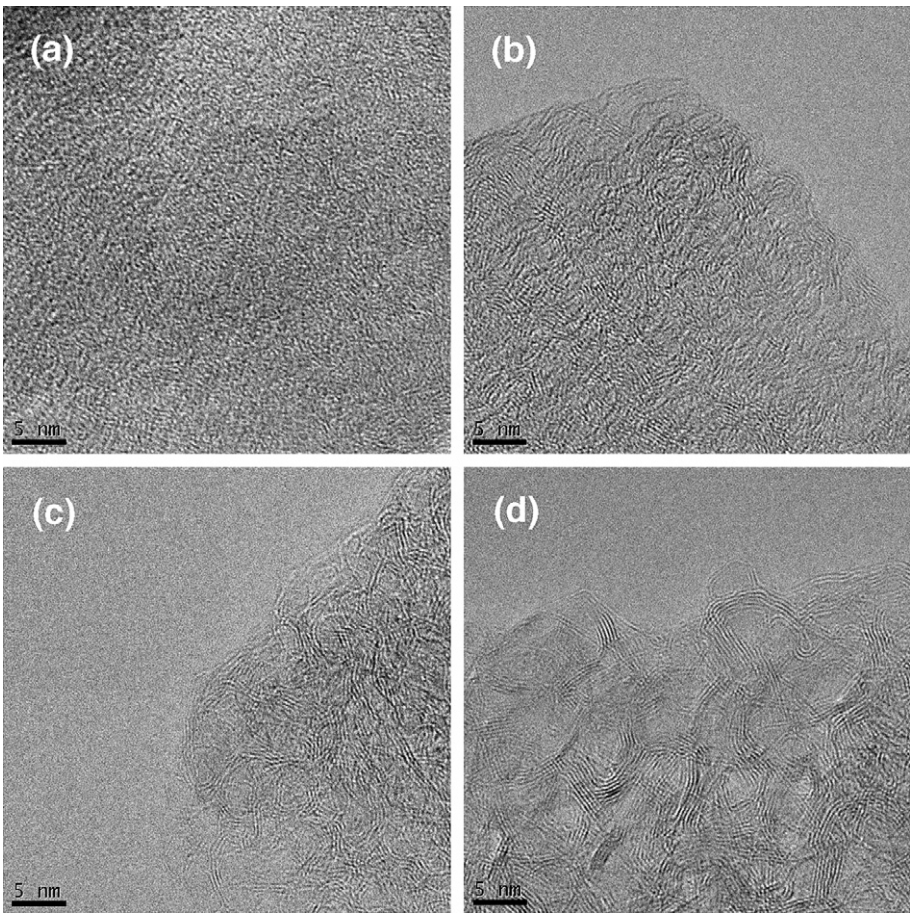

Fig. 4 – TEM images of (a) NPC800, (b) NPC1200, (c) NPC1800 and (d) NPC2000.

ume which could be sustained during HTT. For each of the other activated samples, the mean pore widths were all shifted to 0.82 nm.

Powder diffraction patterns were collected after the various activated carbons were annealed at 2000 °C and they are shown in Fig. 13. The calculated parameters d_{002}, L_c, and L_a are given in Table 3. The (002) reflection characteristic of activated carbon subjected to HTT at 2000 °C was evident in each of the samples. A graphitic peak appeared over the amorphous background after just 15% activation; however, it was not possible to fit both A- and T- peaks. The line was attributed solely to an amorphous carbon. An A- and T-component were distinguishable in the a-NPC2000/42 sample. The annealed carbon initially activated to 69% burnoff also had A- and T-components, but a G-component was also found. The growth of L_a was again analogous to the non-activated samples.

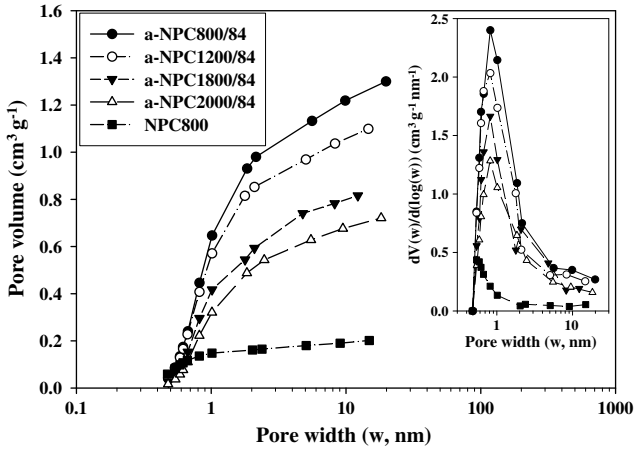

Fig. 5 – Total and differential pore volumes of NPC800, a-NPC800/84, a-NPC1200/84, a-NPC1800/84, and a-NPC2000/84, as calculated by the methyl chloride adsorption isotherm.

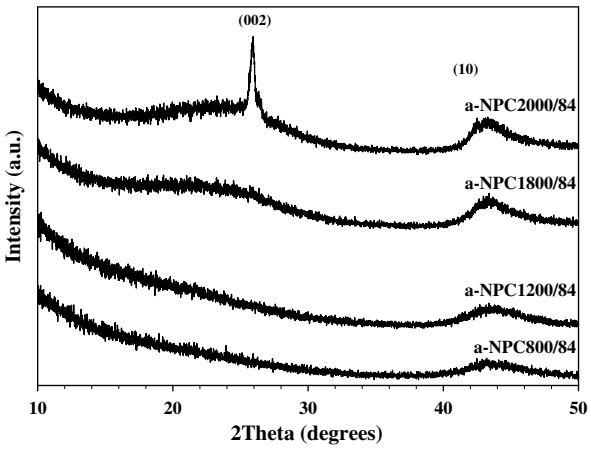

Fig. 6 – XRD patterns of a-NPC/84 as a function of HTT.

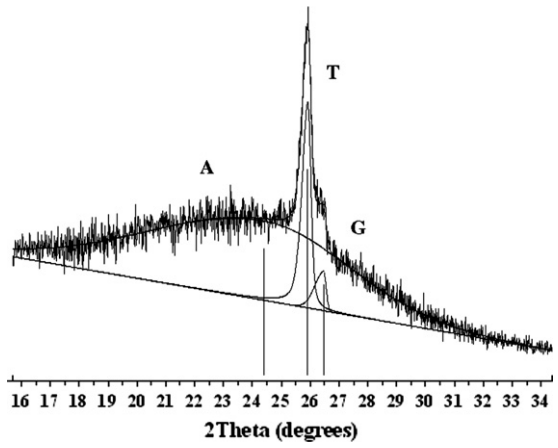

Fig. 7 – Fit of A-, T-, and G-components to a-NPC2000. The d_{002} of the three components were 3.66, 3.44, and 3.37 Å. Crystallite sizes (L_c) were 10, 276, and 145 Å, respectively.

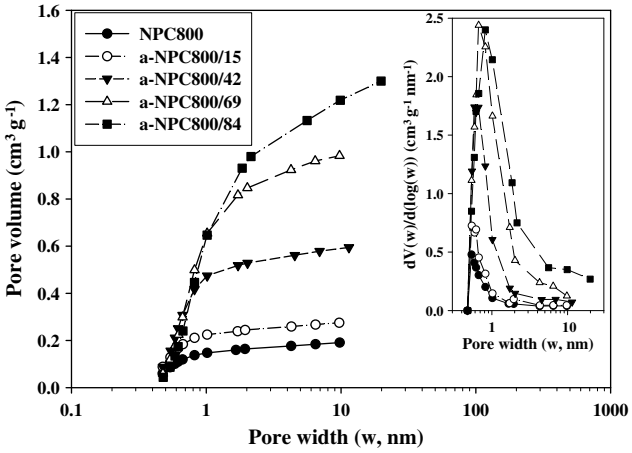

Fig. 9 – Total and differential pore volumes of NPC800 and a-NPC to 15%, 42%, 69%, and 84% burnoff, as calculated by the methyl chloride adsorption isotherm.

4. Discussion

The carbon derived from pyrolysis of polyfurfuryl alcohol is non-graphitizing. Cross-linking in the polymerization of furfuryl alcohol is considered to be the underlying factor which gives rise to the resistance to graphitization these materials display. Yet, how this manifestation of the cross-link structure exerts its influence mechanistically in these carbon materials is unknown. However, the differences between the behavior of native NPC and a-NPC when subjected to HTT up to 2000 °C help to elucidate a previously unknown pathway that now provides for the conversion of a non-graphitizing carbon into a graphitizing carbon. By reducing

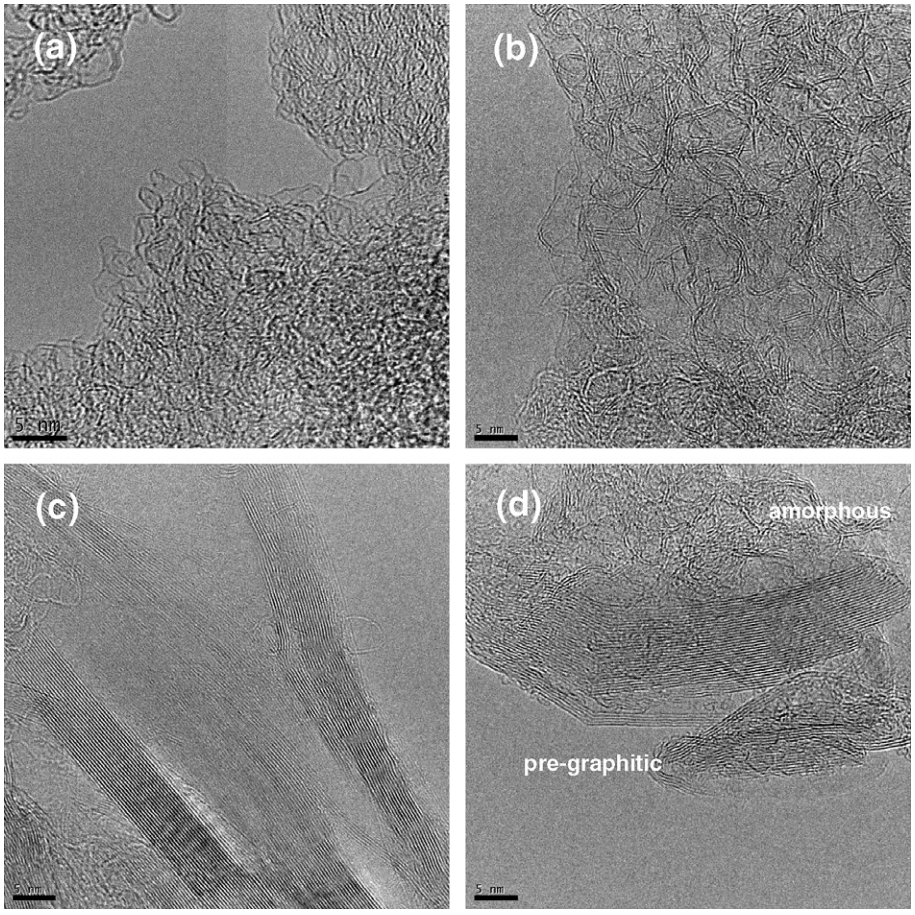

Fig. 8 – TEM images of (a) a-NPC800/84, (b), (c), and (d) a-NPC2000/84.

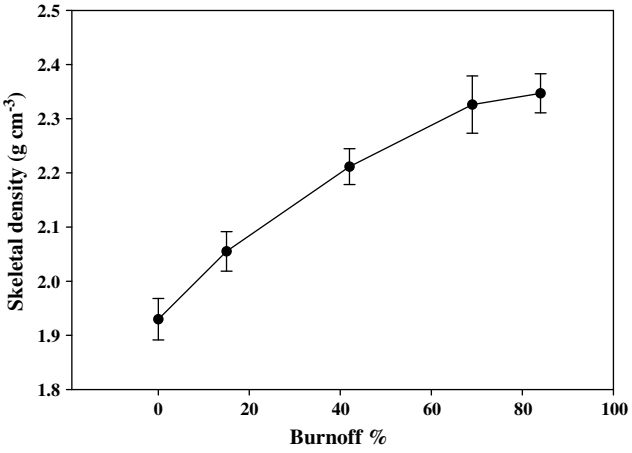

Fig. 10 – Skeletal density of a-NPC activated to 15%, 42%, 69%, and 84% burnoff.

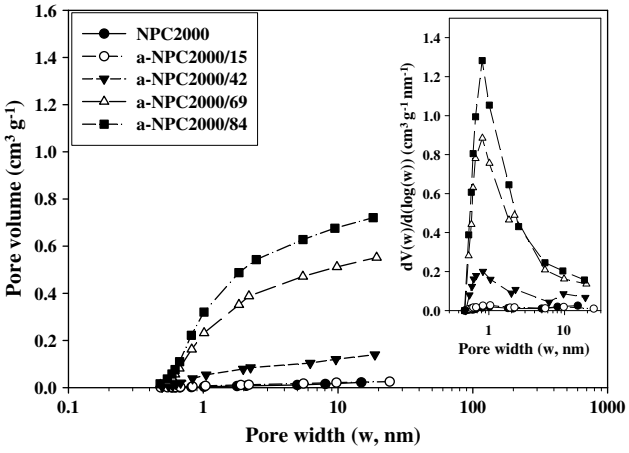

Fig. 12 – Total and differential pore volumes of a-NPC2000 which was previously activated to 0%, 15%, 42%, 69%, and 84% burnoff, as calculated by the methyl chloride adsorption isotherm.

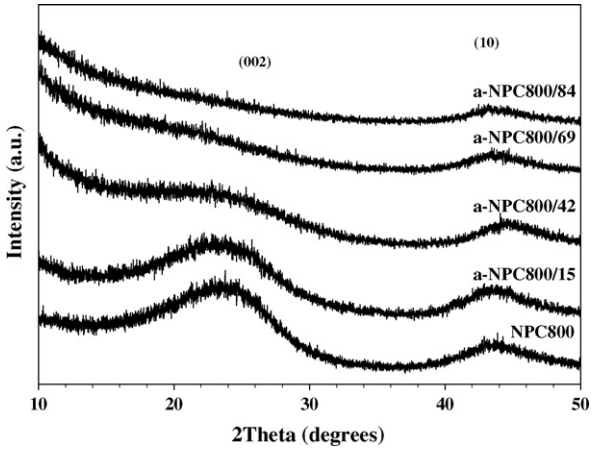

Fig. 11 – XRD patterns of NPC800 and a-NPC800 activated to 15%, 42%, 69%, and 84% burnoff.

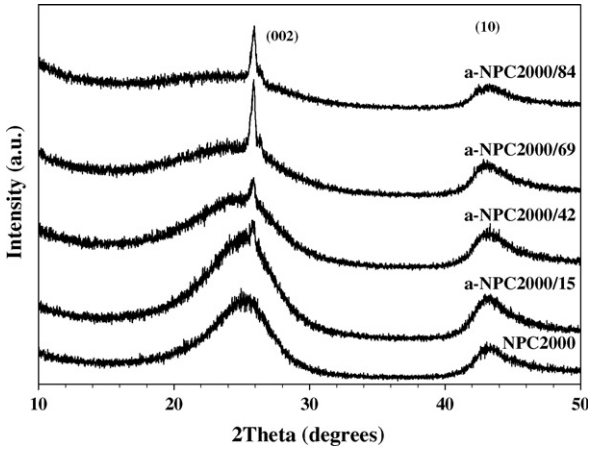

Fig. 13 – XRD patterns of NPC2000 and a-NPC2000, which was activated to 15%, 42%, 69%, and 84% burnoff prior to annealing at 2000 °C.

Table 3 – Interlayer spacing (d_{002}), and crystallite sizes (L_c and L_a) for components of NPC and a-NPC for various activation times

Sample	Component	d_{002} (Å)	L_c (Å)	L_a (Å)
NPC800	A	3.69	10	15
a-NPC800/15	A	3.74	10	16
a-NPC800/42	A	3.70	10	17
a-NPC800/69	A	–	–	16
a-NPC800/84	A	–	–	17
NPC2000	A	3.50	15	27
a-NPC2000/15	A	3.49	14	26
a-NPC2000/42	A	3.54	12	26
	T	3.44	279	
a-NPC2000/69	A	3.60	10	26
	T	3.44	277	
	G	3.38	204	
a-NPC2000/84	A	3.66	10	25
	T	3.44	276	
	G	3.37	145	

L_a was calculated from the (10) peaks.

the barrier to graphitization, this new pathway offers clues that further our understanding of the origin of the thermal stability in the native materials.

NPC800 derived from PFA and Triton X-100 is both nano- and mesoporous. After HTT the accessibility of the probe gas (methyl chloride) to the nanopore structure in NPC1200 is reduced. The nanopore volume falls from 0.16 to 0.04 $cm^3 g^{-1}$. Further annealing at 2000 °C closes all but a small volume of mesopores, 0.02 $cm^3 g^{-1}$. Correspondingly, the apparent surface area of the carbon decreases from 317 to 22 $m^2 g^{-1}$ after HTT.

The skeletal density of a perfect graphite crystal is 2.25 g cm^{-3}. The density of NPC800 is much lower, 1.93 g cm^{-3}. This difference is attributed to both the disordered and defective layers of graphenes and to the presence of closed porosity produced during pyrolysis. Closed pores leave inaccessible void spaces in the carbon structure, which contribute to the apparent volume occupied by the carbon,

but do not increase the mass. Despite the immediate changes in porosity observed after annealing at 1200 °C, the skeletal density of NPC is unchanged up to 1400 °C. Thus the pore structure is not completely closed, rather the pore mouths are narrowed to exclude methyl chloride, but permit entrance of the smaller helium molecule. Annealing above 1400 °C causes complete pore closure to occur and the density decreases to 1.4 g cm^{-3} for NPC2000.

Crystalline graphite is characterized by a sharp (002) diffraction peak at $2\theta = 26.5°$, which corresponds to a d_{002} of 3.35 Å. The X-ray diffraction patterns of NPC annealed up to 2000 °C clearly indicate that polyfurfuryl alcohol derived carbon is non-graphitizing. The crystallinity of NPC1200 is unchanged, but further heating to 1800 and 2000 °C shifts the (002) line towards 26.5° and reduces peak broadening. The d_{002} is decreased to 3.51 Å for NPC2000 and the average L_c size grows from 10 to just 15 Å. Significant stacking of the layer planes does not occur; neither does edge coalescence. The L_a parameter roughly doubles with HTT to 2000 °C.

The local microstructure of the carbons is observed in the TEM. No clear, coherent structures are found in the image of NPC800, Fig. 4a. The graphenes are randomly oriented with respect to each other. A change in the microstructure is evident in Fig. 4b, which corresponds to NPC1200. Small groups of graphenes have coalesced into more ordered structures. The domains of higher crystallinity continue to grow at 1800 °C. NPC2000 is comprised of intertwined ribbons of layered graphenes, Fig. 4d. The ribbons are at most 10 layers thick and are highly curved, which reduces coherence in the *a*-direction. Continuity of the crystallinity in the domains extends only a few nanometers. According to the bulk X-ray pattern, NPC2000 is still considered globally amorphous.

Activation with CO_2 to 84% burnoff greatly increases the pore volume of the carbon. Annealing at 1200 °C causes a 15% drop in porosity. Porosity is further diminished in a-NPC1800/84 and the volume of a-NPC2000/84 is 55% of the original a-NPC800/84. The pore volumes are still significantly larger than those realized prior to activation; recall that for NPC2000 the pore volume is essentially eliminated. An average pore width of 0.82 nm is maintained throughout the HTT for the activated samples. The carbon remains amorphous throughout activation, as shown in Fig. 8a.

If the open pores are converted to closed pores, an accompanying decrease in skeletal density is expected. The skeletal density does linearly decrease with HTT from 2.35 g cm^{-3} for a-NPC800/84 to 1.96 g cm^{-3} for a-NPC2000/84. The 0.39 g cm^{-3} drop in density is accompanied by a 0.58 g cm^{-3} loss of pore volume. Whereas with the non-activated samples a pore volume decrease of 0.17 g cm^{-3} causes a 0.53 g cm^{-3} drop in density. Pore closure is occurring in the activated samples, but not all pores leave behind inaccessible void spaces. The decrease in density is disproportionate to the loss of porosity; therefore a portion of the pores must be converted to a higher density material.

XRD patterns of the annealed activated carbons are remarkably different from those of their non-activated counterparts. A (002) line for a-NPC800/84 in Fig. 6 is undetectable. The intensity of the (002) peak is related to the stacking of graphenes in the layers which form the pore walls. Its absence indicates the pore wall thickness is reduced during activation below the level of detection. The pore walls of the activated carbon are comprised of very few layers or even a single graphene. An HRTEM study on activated saccharose-based chars conducted by Duber et al. also found single layers upon activation [28]. Annealing the carbon causes the graphenes to coalesce and form thicker domains. A broad, low intensity (002) line reappears in a-NPC1800/84. Further HTT to 2000 °C creates a new kind of carbon material since the sharp line at 26° indicates graphitic carbon is present in the sample.

Deconvolution of the a-NPC2000/84 (002), shown in Fig. 7, reveals three components: amorphous (A), turbostratic (T), and graphitic (G) [26,27]. The broad amorphous background peak has a d_{002} of 3.66 Å, which is reminiscent of NPC800 with a 3.68 Å d_{002}. The sharp line at 26° is assigned to turbostratic carbon and the shoulder peak at 26.5° is graphitic carbon. Confirmation of the presence of the three structures is found in the TEM images of Fig. 8. An amorphous region of a-NPC2000 is shown in Fig. 8b. Graphitic and turbostratic morphologies are evident in Fig. 8c. The three components are shown together in Fig. 8d. The ordered structures are termed pre-graphitic as order extends in two dimensions; L_a remains small.

The effect of activation time on the tendency of the carbon to graphitize at 2000 °C was studied by reducing the activation burnoff to several points less than 84%. The slight increase in nanoporosity found after 15% of activation was accompanied by an increase in skeletal density. The initially closed porosity is not yet entirely opened; else the skeletal density would approach 2.25 g cm^{-3}. The entire pore structure must be open before pore wall thinning becomes the dominant activation process. Therefore the (002) peak intensity has not reduced in a-NPC800/15 and graphitization has not occurred after annealing at 2000 °C (a-NPC2000/15). A sharper jump in porosity occurs after 1.5 h of activation and the density reaches 2.22 g cm^{-3}, which is on par with graphite. The entire pore structure is accessible to the probe gas at this point. Additional porosity is now created by pore wall thinning and removal of less stable, disordered carbon. This is evident in the reduction of the (002) line of a-NPC800/42. Oxidation of the pore walls by loss of disordered carbon facilitates formation of pre-graphite, as a turbostratic peak is fit to the XRD pattern of a-NPC2000/42. Continued activation to 69% burnoff further increases nanoporosity, while also introducing mesoporosity. The skeletal density increases to match the 84% sample and the (002) peak is approaching the limit of detection in a-NPC800/69. A G-component is identified after annealing. The final activation primarily generates mesoporosity, but also further thins the nanopore walls, as the (002) line has become indistinguishable from the background. However, activation to 69% sufficiently frees the graphenes to coalesce and form the G-component. HTT at 2000 °C does not eliminate the whole of the nanoporosity for these carbons with one expection – that is a-NPC2000/15, which had an activated pore volume barely larger than a non-activated carbon.

NPC pyrolyzed at 800 °C is non-graphitizing even when annealed at 2000 °C. The carbon is comprised of disordered of graphenes, which are “kinetically frozen” [9]. Although disordered, the layers are interconnected and contain non-six-membered rings which prevent realignment of the layers to

form long-range graphitic structures. Although high temperature treatment between 1200 and 2000 °C is able to progressively introduce further order in the material; it must be considered globally amorphous. The pore structure is rendered completely inaccessible as a result of the effects of the thermally forcing conditions. Activation dramatically enhances the carbon porosity and enables gas molecules access to the entire material. A side effect is the removal of a significant amount of carbon material from the original structure. This is expected to include especially those portions of the highly disordered carbon that contain five and seven-member rings, and which are more susceptible to oxidation than pristine graphenes. A reduction in the number of graphenes in the pore wall is also found via XRD. After removal of a portion of this highly disordered carbon, the thinner layer stacks are more mobile and are able to align themselves into turbostratic domains with long-range order when annealed at 2000 °C. Activation to 42% burnoff is sufficient to permit turbostratic carbon formation. However, an additional activation, 69% or 84% in total, is necessary to adequately thin the layers to permit graphite formation. The domains are not three dimensional, therefore the structures are properly termed pre-graphitic. Conversion to pre-graphite is incomplete and thus nanoporous amorphous carbon remains interspersed with the pre-graphitic structures. This inhomogeneous microstructure is advantageous since it preserves the very useful molecular sieving nanopores, with an average width of 0.82 nm, and these create surface area and provide ready access to the pre-graphitic regions deep within the solid.

5. Conclusions

Rouzaud and Oberlin suggested graphitizing carbons consist of basic structural units which cyrstalltize by passing through four stages during HTT [7]. At each stage sufficient thermal energy is provided to release heteroatoms or to drive out defects in the graphenes. The end result is a highly crystalline graphitic carbon. In the case of non-graphitizing carbons, this process is localized. Highly disordered carbon, which is a legacy of cross-linking in the polymeric phase, restricts the freedom of the basic structural units to align and to form graphite. Activation removes disordered, oxidation-susceptible carbon structures, thereby reducing the barrier to graphitization in polyfurfuryl alcohol derived nanoporous carbon. When activation is followed by annealing at 2000 °C, a portion of the once non-graphitizing carbon is now able to organize into pre-graphitic structures. However, and quite significantly, the nanopores originally present are not completely eliminated after HTT of the a-NPC; this behavior is quite unlike native NPC. The product is a hetergeneous carbon exhibiting both nanoporosity, a property of the non-graphitizing carbon, and pre-graphite, which is a crystalline component.

Acknowledgements

The authors would like to the Materials Research Institute at the Pennsylvania State University for providing characterization equipment and assistance. Partial funding for this research was provided by NSF NIRT-DMR-0304391.

REFERENCES

[1] Franklin R. Crystallite growth in graphitizing and non-graphitizing carbons. Proc R Soc 1951;A209:196–218.
[2] Jenkins GM, Kawamura K. Polymeric carbons. Cambridge: Cambridge University Press; 1976.
[3] Shiflett MB, Foley HC. Ultrasonic deposition of high-selectivity nanoporous carbon membrane. Science 1999;285:1902.
[4] Rajagopalan R, Merritt A, Tseytlin A, Foley HC. Modification of macroporous stainless steel supports with silica nanoparticles for size selective carbon membranes with improved flux. Carbon 2006;44(10):2051–8.
[5] Merritt A, Rajagopalan R, Foley HC. High performance nanoporous carbon membranes for air separation. Carbon 2007;45(6):1267–78.
[6] Rajagopalan R, Ponnaiyan A, Mankidy PJ, Brooks AW, Yi B, Foley HC. Molecular sieving platinum nanoparticle catalysts kinetically frozen in nanoporous carbon. Chemical Commun 2004:2498–9.
[7] Foley HC. Carbogenic molecular sieves: synthesis, properties and applications. Microporous Mater 1995;4:407–33.
[8] Fitzer E, Schafer W. The effect of crosslinking on the formation of glasslike carbons from thermosetting resins. Carbon 1970;8:353–64.
[9] Mariwala RK, Foley HC. Evolution of ultramicroporous adsorptive structure in poly(furfuryl alcohol)-derived carbogenic molecular sieves. Ind Eng Chem Eng 1994;33:607–15.
[10] Burket CL, Rajagopalan R, Marencic A, Dronavajjala K, Foley HC. Genesis of porosity in polyfurfuryl alcohol derived nanoporous carbon. Carbon 2006;44(14):2957–63.
[11] Rouzaud JN, Oberlin A. Structure, microtexture, and optical properties of anthracene and saccharose-based carbons. Carbon 1989;27(4):517–29.
[12] Dahn JR, Xing W, Gao Y. The "falling cards model" for the structure of microporous carbons. Carbon 1997;35(6):825–30.
[13] Harris PJF, Tsang SC. High-resolution electron microscopy studies of non-graphitizing carbons. Philos Mag A 1997;76(3):667–77.
[14] Harris PJF. Fullerene-related structure of commercial glassy carbons. Philos Mag 2004;84(29):3159–67.
[15] Acharya M, Strano MS, Mathews JP, Billinge SJL, Petkov V, Subramoney S, et al. Simulation of nanoporous carbons: a chemically constrained structure. Philos Mag B 1999;79(10):1499–518.
[16] Petkov V, DiFrancesco RG, Billinge SJL. Local structure of nanoporpous carbons. Philos Mag B 1999;79(10):1519–30.
[17] Smith MA, Foley HC, Lobo RF. A simple model describes the PDF of a non-graphitizing carbon. Carbon 2004;42:2041–8.
[18] Jenkins RG, Walker PL. Small-angle X-ray-scattering studies on carbons derived from polyfurfuryl alcohol and polyfurfuryl alcohol-ferrocene copolymers. Carbon 1976;14(1):7–11.
[19] Oya A, Mochizuki M, Otani S, Tomizuka I. Electron-microscopic study on the turbostratic carbon formed in phenolic resin carbon by catalytic action of finely dispersed nickel. Carbon 1979;17(1):71–6.
[20] Oya A, Otani S. Catalytic graphitization of carbons by various metals. Carbon 1979;17(2):131–7.
[21] Marsh H, Crawford D, Taylor DW. Catalytic graphitization by iron of isotropic carbon from polyfurfuryl alcohol, 725–1090 K – a high-resolution electron-microscope study. Carbon 1983;21(1):81–7.
[22] Franklin RE. Homogeneous and heterogeneous graphitization of carbon. Nature 1956;177(4501):239.

[23] Honda H, Kobayash K, Sugawara S. X-ray characteristics of non-graphitizing-type carbon. Carbon 1968;6(4):517–23.
[24] Mariwala RK, Foley HC. Calculation of micropore sizes in carbogenic materials from the methyl chloride adsorption isotherm. Ind Eng Chem Eng 1994;33(10):2314–21.
[25] Maggs FAP, Schwabe PH, Williams JH. Adsorption of helium on carbons: influence on measurement of density. Nature 1960;186:956–8.
[26] Oya A, Marsh H. Review: phenomena of catalytic graphitization. J Mater Sci 1982;17:309–22.
[27] Honda H, Kobayashi K, Sugawara S. X-ray characteristics of non-graphitizing-type carbon. Carbon 1967;6:517–23.
[28] Duber S, Rouzaud J-N, Clinard C, Pusz S. Microporosity and optical properties of some activated chars. Fuel Process Technol 2002;77–78:221–7.